Eur. Phys. J. B **11**, 407–421 (1999)

THE EUROPEAN PHYSICAL JOURNAL B

EDP Sciences

Influence of carrier correlations on the excitonic optical response including disorder and microcavity effects

C. Sieh, T. Meier[a], A. Knorr, F. Jahnke, P. Thomas, and S.W. Koch

Department of Physics and Material Sciences Center, Philipps University, Renthof 5, 35032 Marburg, Germany

Received 22 January 1999

Abstract. A model study of the characteristic signatures of carrier-correlation effects on the excitonic differential absorption spectra in semiconductors is presented. Using an effectively one-dimensional tight-binding system Coulomb-induced carrier-correlations up to third-order in the optical field are treated without additional approximations. To illustrate the influence of the different many-body contributions excitonic differential absorption spectra are computed for various polarizations and pump-probe time delays. The simultaneous influence of energetic disorder and correlations on the differential absorption spectra is discussed. Also presented are numerical results for the case when the semiconductor system is placed inside a microcavity in the strong-coupling regime. It is shown that the correlations induce characteristic signatures in the normal mode spectra.

PACS. 71.35.Cc Intrinsic properties of excitons; optical absorption spectra – 42.50.Md Optical transient phenomena: quantum beats, photon echo, free-induction decay, dephasings and revivals, optical nutation, and self-induced transparency – 78.66.-w Optical properties of specific thin films, surfaces, and low-dimensional structures: superlattices, quantum well structures, multilayers, and microparticles

1 Introduction

The recent progress in experimental techniques and resolution requires an improved level of theoretical analysis of the nonlinear optical response of semiconductors and semiconductor nanostructures. In particular, it is interesting and necessary to investigate Coulomb-induced carrier correlations, *i.e.* terms in the many-body hierarchy which go beyond the time-dependent Hartree-Fock approximation [1–14]. In particular the polarization-dependence of the nonlinear optical response has been interpreted in terms of excitation-induced dephasing processes [1,2]. Furthermore, signatures of bound [3,6–12] and unbound two-exciton states [3] were investigated both theoretically and experimentally.

Previous work on higher-order correlation effects has often focussed on time-domain four-wave mixing, where the field emitted into a background free direction is analyzed, see reference [3] and references therein. Only few publications exist which study the effects of carrier-correlations on pump-probe type (differential absorption/transmission) experiments [5,14–18] and a detailed microscopic theoretical study on the influence of carrier-correlations on polarization-dependent differential absorption spectra is still missing. As far as the description of disorder effects on the $\chi^{(3)}$-processes beyond the Hartree-Fock level is concerned, only some phenomenological approaches are available [12,19], but no consistent microscopic treatment has been reported so far.

The development of high-quality microcavities has opened up new possibilities for studying light-matter interaction. In the so-called strong-coupling regime, the splitting of the eigenstates of the absorber and cavity modes (normal-mode splitting), has been predicted [20] and observed in atomic [21] and semiconductor [22] systems. The nonlinear saturation of excitonic normal-mode coupling after femtosecond-pulse excitation has been studied [23,24], and time-integrated [25] or time-resolved [26] four-wave mixing have been analyzed. Recently, polarization-dependent changes of the normal mode splitting have been observed in pump-probe type differential reflection experiments [27].

In this paper we present a detailed analysis of carrier-correlation effects on differential absorption spectra within the coherent $\chi^{(3)}$-limit [3,4,14]. The energies and oscillator strengths of bound and unbound two-exciton states are computed consistently on a microscopic basis. Furthermore, we analyze disorder effects by treating the influence of disorder and correlations simultaneously. The dependence of the differential absorption spectra on the polarization geometry of the incident pulses and their time-delay is discussed and the effects induced by energetic disorder are analyzed for the polarization-dependent differential absorption spectra. Finally, the configuration of the excitonic system inside a microcavity is analyzed for the case where the exciton energy is in resonance

[a] e-mail: torsten.meier@physik.uni-marburg.de

with the optical cavity mode. The polarization dependence of the normal mode splitting [27] and additional signatures in the pump-probe reflection spectra are discussed.

The paper is organized as follows: In Section 2 the theoretical approach is presented and the general equations determining the optical response within the coherent $\chi^{(3)}$-limit are given. In Section 3 the one-dimensional model is introduced for which the coupled equations are numerically evaluated. Results for excitonic differential absorption spectra including carrier-correlations are presented and discussed in Section 4. Important features of the numerical results are analyzed on the basis of an analytical solvable model system introduced in Appendix A. The consequences of energetic disorder are discussed in Section 5. Numerical results for the differential reflection spectra of a microcavity are presented in Section 6. Our results are summarized in Section 7.

2 Theoretical approach

We use the Hamiltonian:

$$H = H_0 + H_{\mathrm{C}} + H_{\mathrm{I}}, \tag{1}$$

where H_0 is the single-particle Hamiltonian, H_{C} the Coulomb interaction, and H_{I} the interaction with a classical electric field.

The single-particle Hamiltonian H_0 reads:

$$H_0 = \sum_{ijc} T^c_{ij} a_i^{c+} a_j^c + \sum_{ijv} T^v_{ij} a_i^{v+} a_j^v. \tag{2}$$

Here, i and j refer to real-space sites, and c (v) label the conduction (valence) bands. a_i^{c+} (a_j^c) creates (destroys) an electron at site i (j) in band c, and a_i^{v+} (a_j^v) creates (destroys) a hole at site i (j) in band v. The diagonal terms of the matrices T contain the electronic site energies and the couplings between the sites define the off-diagonal matrix elements.

We use the Coulomb Hamiltonian H_{C} in the form:

$$H_{\mathrm{C}} = \frac{1}{2} \sum_{ijcvc'v'} (a_i^{c'+} a_i^{c'} - a_i^{v'+} a_i^{v'}) V_{ij} (a_j^{c+} a_j^c - a_j^{v+} a_j^v), \tag{3}$$

where V_{ij} describes the monopole-monopole [28] Coulomb interactions between particles at sites i and j. The dipole interaction of the electronic system with a classical electric field is given by:

$$H_{\mathrm{I}} = -\mathbf{E}(t) \cdot \mathbf{P} = -\mathbf{E}(t) \cdot \sum_{ijvc} (\boldsymbol{\mu}^{vc}_{ij} a_i^v a_j^c + (\boldsymbol{\mu}^{vc}_{ij})^* a_j^{c+} a_i^{v+}), \tag{4}$$

where $\boldsymbol{\mu}$ is the matrix element for the optical transition between the valence and conduction bands and $\mathbf{P}$ is the optical interband polarization.

Using the total Hamiltonian H, the equation of motion of the interband coherence $p^{v_1c_2}_{12} = \langle a_1^{v_1} a_2^{c_2} \rangle$ is obtained as:

$$\begin{aligned}
-\mathrm{i}\partial_t p^{v_1c_2}_{12} =& -\sum_j T^c_{2j} p^{v_1c_2}_{1j} - \sum_i T^v_{i1} p^{v_1c_2}_{i2} + V_{12} p^{v_1c_2}_{12} \\
&- \mathbf{E}(t) \cdot [(\boldsymbol{\mu}^{v_1c_2}_{12})^* - \sum_{jc} (\boldsymbol{\mu}^{v_1c}_{1j})^* f^{cc_2}_{j2} - \sum_{iv} (\boldsymbol{\mu}^{vc_2}_{i2})^* f^{vv_1}_{i1}] \\
&+ \sum_{av_a} V_{a1} \langle a_a^{v_a} a_1^{v_1} a_a^{v_a+} a_2^{c_2} \rangle - \sum_{av_a} V_{2a} \langle a_1^{v_1} a_a^{v_a} a_2^{c_2} a_a^{v_a+} \rangle \\
&+ \sum_{ac_a} V_{a1} \langle a_a^{c_a+} a_1^{v_1} a_a^{c_a} a_2^{c_2} \rangle - \sum_{ac_a} V_{2a} \langle a_1^{v_1} a_a^{c_a+} a_2^{c_2} a_a^{c_a} \rangle.
\end{aligned} \tag{5}$$

Here we have introduced the electron and hole populations and intraband coherences which are defined as $f^{cc_2}_{j2} = \langle a_j^{c+} a_2^{c_2} \rangle$ and $f^{v_1v}_{1i} = \langle a_1^{v_1+} a_i^v \rangle$, respectively. The four-point correlation functions represent the first step of the infinite hierarchy of many-particle correlations induced by the Coulomb interaction.

In this paper, we consider the coherent limit in which dephasing processes due to scattering with other quasiparticles is neglected. Furthermore, we assume relatively weak excitation intensities and include only terms which contribute to the optical response up to third-order in the optical field. Within these assumptions the electron and hole populations and coherences do not have to be treated as independent variables but can be expressed *via* the interband coherences p using [4,14]

$$\sum_{av_a} p^{v_ac_2}_{a2} (p^{v_ac_1}_{a1})^* = f^{c_1c_2}_{12}, \tag{6}$$

and

$$\sum_{ac_a} p^{v_1c_a}_{1a} (p^{v_2c_a}_{2a})^* = f^{v_1v_2}_{12}. \tag{7}$$

Similarly, the four-point terms appearing in equation (5) can written as [4,14]

$$\langle a_a^{v_a+} a_1^{v_1} a_a^{v_a} a_2^{c_2} \rangle = \sum_{bc_b} \langle a_1^{v_1} a_b^{c_b} a_a^{v_a} a_2^{c_2} \rangle (p^{v_ac_b}_{ab})^*. \tag{8}$$

Applying this decoupling scheme to all terms in equation (5) the optical response up to $\chi^{(3)}$ can be expressed using two transition-type quantities. These are the interband coherences $p^{v_1c_2}_{12}$ related to single-excitons and $\sigma^{v_1vcc_2}_{1234} = \langle a_1^{v_1} a_2^v a_3^c a_4^{c_2} \rangle$, which describes two-exciton excitations [3,4,14]. In order to be able to analyze pure correlation effects, which go beyond the time-dependent Hartree-Fock approximation [29], it is advantageous to remove the uncorrelated parts from the four-point quantities σ, *i.e.* to define [3]

$$\bar{\sigma}^{v_1vcc_2}_{1234} = \sigma^{v_1vcc_2}_{1234} - p^{v_1c_2}_{14} p^{vc}_{23} + p^{v_1c}_{13} p^{vc_2}_{24}. \tag{9}$$

This procedure results in closed equations of motion for the single-exciton amplitude p^{vc}_{12} and the two-exciton amplitude $B^{v_1cvc_2}_{1324} \equiv -\bar{\sigma}^{v_1vcc_2}_{1234}$, which completely determine

the optical response within the coherent $\chi^{(3)}$ limit [3,4,14]. The equation of motion for p is then obtained as:

$$\begin{aligned} -\ \mathrm{i}\ \partial_t p^{vc}_{12} &= -\sum_j T^c_{2j} p^{vc}_{1j} - \sum_i T^v_{i1} p^{vc}_{i2} + V_{12} p^{vc}_{12} \\ &+ \sum_{abv'c'} (V_{a2} - V_{a1} - V_{b2} + V_{b1})[(p^{v'c'}_{ba})^* p^{v'c}_{b2} p^{vc'}_{1a} \\ &- (p^{v'c'}_{ba})^* p^{v'c'}_{ba} p^{vc}_{12} - (p^{v'c'}_{ba})^* B^{v'c'vc}_{ba12}] \\ &+ \mathbf{E}(t) \cdot [(\boldsymbol{\mu}^{vc}_{12})^* - \sum_{abv'c'} ((\boldsymbol{\mu}^{vc'}_{1b})^* (p^{v'c'}_{ab})^* p^{v'c}_{a2} \\ &+ (\boldsymbol{\mu}^{v'c}_{b2})^* (p^{v'c'}_{ba})^* p^{vc'}_{1a})]. \end{aligned} \tag{10}$$

Here, the first line gives the homogeneous part of the equation of motion, which includes the electronic energies and couplings (T) and the electron-hole Coulomb attraction (V_{12}). The following lines describe different types of inhomogeneities. In addition to the linear source term given by the external field times the dipole transition matrix element, $\mathbf{E}(t) \cdot \boldsymbol{\mu}^*$, in the coherent $\chi^{(3)}$ limit there are the optical nonlinearities arising from Pauli-blocking (also called phase-space filling) ($\mu^* E p^* p$) and from the many-body Coulomb interaction. The latter include the first-order Coulomb contribution ($V p^* pp$) and the correlation contribution ($V p^* B$) [3]. The nonlinear response can be written as a sum over the contributions from these three types of optical nonlinearities, which makes it possible to investigate them separately [3,5,13].

The second term $\propto p^{v'c'*}_{ba} p^{v'c'}_{ba} p^{vc}_{12}$ in line two of equation (10) looks like an energy renormalization. Using the typical selection rules for heavy-hole to conduction electron (hh-e) transitions [3,9], this term, which is of first-order in the Coulomb interaction, introduces a coupling between the spin subspaces. This term vanishes only in a homogeneous system, in inhomogeneous, for example disordered systems, it is finite and contributes to the nonlinear response.

The equation of motion for B is obtained as

$$\begin{aligned} -\ \mathrm{i}\ \partial_t B^{v'c'vc}_{ba12} &= -\sum_i (T^c_{2i} B^{v'c'vc}_{ba1i} + T^v_{i1} B^{v'c'vc}_{bai2} \\ &+ T^c_{ai} B^{v'c'vc}_{bi12} + T^v_{ib} B^{v'c'vc}_{ia12}) \\ &+ (V_{ba} + V_{b2} + V_{1a} + V_{12} - V_{b1} - V_{a2}) B^{v'c'vc}_{ba12} \\ &- (V_{ba} + V_{12} - V_{b1} - V_{a2}) p^{vc'}_{1a} p^{v'c}_{b2} \\ &+ (V_{1a} + V_{b2} - V_{b1} - V_{a2}) p^{v'c'}_{ba} p^{vc}_{12}. \end{aligned} \tag{11}$$

The first three lines in equation (11) constitutes the homogeneous part of the equation of motion, which includes the electronic energies and couplings (T) as well as the six possible Coulomb-interactions between the two electrons and the two holes. The last two lines in equation (11) represent the inhomogeneities. Since the uncorrelated first-order Coulomb contributions have been removed from B it is purely driven by sources which include the many-body interaction V [3,5], *i.e.* by terms proportional to Vpp.

The total interband polarization $\mathbf{P}$ measured in an optical experiment is:

$$\mathbf{P} = \sum_{ijvc} \boldsymbol{\mu}^{vc}_{ij} p^{vc}_{ij}. \tag{12}$$

Equations (10, 11) fully determine the interband polarization $\mathbf{P}$ within the coherent $\chi^{(3)}$ limit [3,4,13,14]. For a spatially homogeneous system the complexity of solving these equations can be reduced, since in this case the center of mass motion is irrelevant. Then p and B depend only on the relative motion of the particles which leads to the k-space equations in [3]. However, in spatially inhomogeneous (for example disordered) systems the complete equations (10, 11) have to be solved. Furthermore these equations can be easily extended to include propagation effects [30].

Instead of removing the uncorrelated parts from the four-point functions, one can also derive equations which describe the optical response up to $\chi^{(3)}$ using the original four-point functions [14]; *i.e.* we can use

$$\tilde{B}^{v_1 c v c_2}_{1324} \equiv -\sigma^{v_1 v c c_2}_{1234} \equiv -\langle a^{v_1}_1 a^v_2 a^c_3 a^{c_2}_4 \rangle. \tag{13}$$

This results in the following equations for p and $\tilde{B}$:

$$\begin{aligned} -\ \mathrm{i}\ \partial_t p^{vc}_{12} &= -\sum_j T^c_{2j} p^{vc}_{1j} - \sum_i T^v_{i1} p^{vc}_{i2} + V_{12} p^{vc}_{12} \\ &- \sum_{abv'c'} (V_{a2} - V_{a1} - V_{b2} + V_{b1})[(p^{v'c'}_{ba})^* \tilde{B}^{v'c'vc}_{ba12}] \\ &+ \mathbf{E}(t) \cdot [(\boldsymbol{\mu}^{vc}_{12})^* - \sum_{abv'c'} ((\boldsymbol{\mu}^{vc'}_{1b})^* (p^{v'c'}_{ab})^* p^{v'c}_{a2} \\ &+ (\boldsymbol{\mu}^{v'c}_{b2})^* (p^{v'c'}_{ba})^* p^{vc'}_{1a})] \end{aligned} \tag{14}$$

and

$$\begin{aligned} -\ \mathrm{i}\ \partial_t \tilde{B}^{v'c'vc}_{ba12} &= -\sum_i (T^c_{2i} \tilde{B}^{v'c'vc}_{ba1i} + T^v_{i1} \tilde{B}^{v'c'vc}_{bai2} \\ &+ T^c_{ai} \tilde{B}^{v'c'vc}_{bi12} + T^v_{ib} \tilde{B}^{v'c'vc}_{ia12}) \\ &+ (V_{ba} + V_{b2} + V_{1a} + V_{12} - V_{b1} - V_{a2}) \tilde{B}^{v'c'vc}_{ba12} \\ &- \mathbf{E}(t) \cdot \Big[(\boldsymbol{\mu}^{vc}_{12})^* p^{v'c'}_{ba} + (\boldsymbol{\mu}^{v'c'}_{ba})^* p^{vc}_{12} \\ &- (\boldsymbol{\mu}^{vc'}_{1a})^* p^{v'c}_{b2} - (\boldsymbol{\mu}^{v'c}_{b2})^* p^{vc'}_{1a} \Big]. \end{aligned} \tag{15}$$

Equations (14, 15) are equivalent to equations (10, 11), *i.e.* solving either one of these equation pairs gives exactly the same result (which has also been verified numerically). What is, however, different, is the appearance of the many-body Coulomb-induced optical nonlinearities in the equation of p. Whereas in equations (10, 11) the Coulomb terms are split into a first-order ($V p^* pp$) and a correlation part ($V p^* B$), no such distinction appears in equations (14, 15), but all many-body nonlinearities are proportional to $V p^* \tilde{B}$.

The comparison of equations (10, 11) and equations (14, 15) indicates that strong compensations between the first-order and the higher-order Coulomb-correlations can be expected. Examples of such cancellations have been reported in reference [23] and can be confirmed by our analytical results in Appendix A and numerical results presented below. As another difference between equations (11, 15), B is driven by inhomogeneous terms proportional to Vpp [3] whereas $\tilde{B}$ is driven by μEp [14]. Therefore the phenomenological approaches used to include two-exciton states in references [9,11,12] are more closely related to equations (14, 15).

At this point it is instructive to compare the discussed approach with the second-order Born approximation (SBA) for the Coulomb interaction [3,23]. The SBA has been successfully applied for excitation conditions where a correlated electron-hole plasma dominates the nonlinear response. In this case, the SBA is valid beyond the $\chi^{(3)}$-regime and includes also the effect of screening of the Coulomb interaction. For a comparison with the treatment of excitonic and biexcitonic correlations discussed in this paper, the SBA has to be combined with a Markov approximation, screening has to be neglected, and only terms up to third order in the optical field have to be retained. At this level, the same equations are obtained if one neglects the Coulomb-terms in the homogeneous part of the equation for B, *i.e.* the third line in equation (11), and solves the resulting equation in Markov approximation. Since the remaining driving terms in the B-equation are proportional to V and B entering in equation (10) is multiplied with V, the resulting contributions in the polarization equation are of second-order in the Coulomb potential.

Hence, the SBA does not include bound two-exciton states and the unbound two-exciton continuum which can strongly influence the optical response if excitons are resonantly excited and plasma excitation is avoided. Furthermore, the Markov approximation appears to be critical under these conditions. In the numerical treatment discussed in this paper, contributions of two-exciton states are fully included on the $\chi^{(3)}$-level *via* the Coulomb-terms appearing in the homogeneous part of the equations for B and the Markov approximation is not used since, in addition to the polarization equation for p, an independent differential equation for B is solved.

3 One-dimensional model

To keep the numerical complexity within reasonable limits, in this paper we concentrate on a one-dimensional model system. Here, the electronic coupling is described in the tight-binding approximation, *i.e.* $T_{ij}^{c,v} = 0$ for $|i-j| > 1$. The diagonal parts $T_{ii}^{c,v} = \epsilon_{c,v} = E_{\mathrm{g}}/2$ are the energies of the electron and hole sites, respectively. Without disorder these energies are taken to be site independent and equal to half the band-gap energy E_{g}. In our study of disorder effects we introduce uncorrelated Gaussian diagonal disorder where the site energies, which vary in an uncorrelated way, are chosen from independent Gaussian distributions.

The tight-binding coupling is described by the off-diagonal elements $T_{i,i+1}^{c,v} = T_{i+1,i}^{c,v} = J_{c,v}$. For the electronic coupling we use $J_c = 15$ meV and for the (heavy-) hole coupling $J_v = 1.5$ meV. The Coulomb-interaction is given by a regularized potential:

$$V_{ij} = U_0 \frac{d}{|i-j|d + a_0},$$

where d is the distance between the sites and U_0 and a_0 are parameters characterizing the strength of the interaction and the spatial variation. In our numerical study we use $U_0 = 15$ meV, $a_0 = 25$ Å, and $d = 50$ Å. Such parametrizations of the Coulomb potential given by equation (3) have been used in describing semiconductor quantum wires [31], in simplified descriptions of superlattices [32], and in analyzing disorder-induced effects in one-dimensional semiconductors [33].

The numerical calculations are performed for a system consisting of 10 sites [34] using periodic boundary conditions. With the above given parameters we obtain an exciton binding energy of 15.1 meV. Furthermore, phenomenological decay times are inserted into the equations of motion. For p we use $\gamma_p^{-1} = 3$ ps and for B $\gamma_B^{-1} = 1.5$ ps, which yields a homogeneous broadening much smaller than the energy difference between the relevant states.

For simplicity we neglect the light-holes and consider two valence and two conduction bands. For the valence bands we include the two degenerate heavy-hole bands, which are characterized by the states $|-3/2h\rangle$ and $|3/2h\rangle$ [3,9]. The two degenerate conduction bands are characterized by $|-1/2e\rangle$ and $|1/2e\rangle$. We assume that the light is propagating in the z-direction and use the usual dipole matrix elements [3,9]:

$$\begin{aligned}
\boldsymbol{\mu}_{ij}^{11} &= \delta_{ij}\mu_0\boldsymbol{\sigma}^{+} = \delta_{ij}\frac{\mu_0}{\sqrt{2}}\begin{pmatrix}1\\ \mathrm{i}\end{pmatrix},\\
\boldsymbol{\mu}_{ij}^{12} &= \boldsymbol{\mu}_{ij}^{21} = 0,\\
\boldsymbol{\mu}_{ij}^{22} &= \delta_{ij}\mu_0\boldsymbol{\sigma}^{-} = \delta_{ij}\frac{\mu_0}{\sqrt{2}}\begin{pmatrix}1\\ -\mathrm{i}\end{pmatrix},
\end{aligned} \tag{16}$$

where μ_0 is the modulus of $\boldsymbol{\mu}$. Consistent with the tight-binding description the optical transitions are assumed to be diagonal in the site index. Furthermore, the typical selection rules for zinc blende semiconductors are used, *i.e.* circularly polarized allowed transitions $|3/2h\rangle \rightarrow |1/2e\rangle$ ($\boldsymbol{\mu}_{ij}^{11}$) and $|-3/2h\rangle \rightarrow |-1/2e\rangle$ ($\boldsymbol{\mu}_{ij}^{22}$). Due to these selection rules we have two separate subspaces of states, which are optically isolated but coupled by the many-body Coulomb-interaction.

For small systems the above discussed equations for p and B can be solved numerically without further approximations. For a schematical drawing of the transitions described by the present model see Figure 1.

Considering an excitation with two optical pulses and using the usual Fourier-expansion with respect

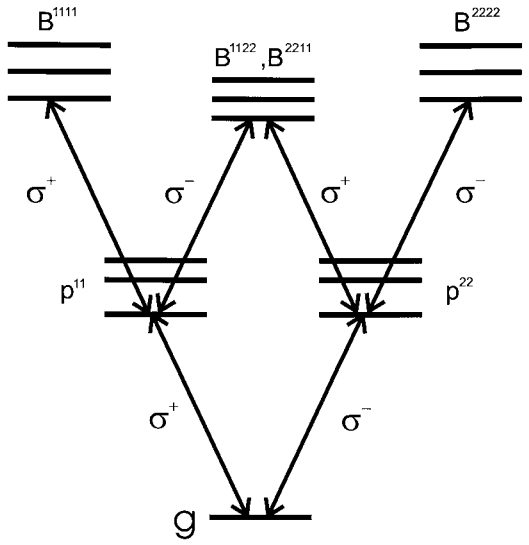

Fig. 1. Schematical drawing of relevant dynamic variables. p is the interband (single-exciton) coherence and B the two-exciton amplitude. The superscripts label the involved electron and hole bands. For further explanation see text.

to the pulse-directions [35] pump-probe and four-wave mixing signals can be obtained. In first-order in the light field only p^{11} and p^{22} can be excited. This is due to the fact that the optical matrix elements for p^{12} and p^{21} vanish and that in in the linear regime no coupling between the subspaces of different spin states exists within our model.

In second-order in the light field, depending on the polarization of the incident laser pulses, different types of two-exciton states can be excited. If we consider two interactions with two co-circularly polarized pulses, then B^{1111} or B^{2222} are relevant. $B^{v'c'vc}_{abcd}$ is antisymmetric with respect to interchanging the band and real-space indices of the two electrons and the two holes, respectively, *i.e.* $B^{vc'v'c}_{cbad} = B^{v'cvc'}_{adcb} = -B^{v'c'vc}_{abcd}$. Since the contributions of the two electrons and the two holes which enter into B^{1111} and B^{2222} come from the same bands, the real-space part of the corresponding B's has to be antisymmetric. Such two-exciton states typically do not include bound states [3,9,14]. If we consider two interactions with oppositely circularly polarized pulses, then B^{1122} and B^{2211} are created in second-order. For these B's no definite symmetry for the real-space part of B exists, and therefore the real-space part may be symmetric which does allow for bound two-exciton states (biexcitons). In the numerical treatment it is sufficient to calculate only one B-term, since the value of the other one can be determined using the anti-symmetry $B^{1122}_{abcd} = B^{2211}_{cdab}$.

Due to the selection rules also in third-order p^{12} and p^{21} do not contribute to the optical response and therefore within $\chi^{(3)}$ the response is fully determined by p^{11} and p^{22}. If equations (10, 11) are projected onto a few relevant single- and two-exciton states it is possible to derive analytical formulae for the resonant nonlinear optical response [3]. In Appendix A this is outlined for a calculation of the differential absorption signals. This analysis gives insight into the signatures of the different optical nonlinearities in the differential absorption spectra.

4 Numerical results for the homogeneous system

We assume excitation with two pulses and use the rotating wave approximation

$$\mathbf{E}(t) = E_1(t)\mathbf{e}_1 \mathrm{e}^{\mathrm{i}(\mathbf{k_1}\cdot\mathbf{r}-\omega_1 t)} + E_2(t)\mathbf{e}_2 \mathrm{e}^{\mathrm{i}(\mathbf{k_2}\cdot\mathbf{r}-\omega_2 t)}. \quad (17)$$

Here $E_1(t) \propto \mathrm{e}^{-((t+\tau)/\bar{t}_1)^2}$ ($E_2(t) \propto \mathrm{e}^{-(t/\bar{t}_2)^2}$) denotes the temporal envelope of the Gaussian pump (probe) pulse which is centered at $t = -\tau$ ($t = 0$), $\mathbf{e}_1$ ($\mathbf{e}_2$) its polarization direction, and ω_1 (ω_2) the central frequency. A positive time delay τ corresponds to the pump pulse arriving before the probe pulse. Equations (10, 11) are solved numerically in the time-domain up to third-order in the optical field ($\chi^{(3)}$). We then obtain $\delta\mathbf{P}(t,\tau)$ [29,36], which is the time-domain polarization in differential absorption geometry, by considering all contributions which (i) propagate in the direction of the probe pulse ($\mathbf{E}_2$), and (ii) include two interactions with the pump pulse ($\mathbf{E}_1$) and are linear in the probe pulse. Since the probe pulse is taken to be spectrally broad the differential absorption can be determined *via*

$$\delta\alpha(\omega,\tau) \propto \mathrm{Im}\left[\int \mathrm{d}t(\mathbf{e}_2)^* \cdot \delta\mathbf{P}(t,\tau)\mathrm{e}^{\mathrm{i}\omega t}\right], \quad (18)$$

where $\mathbf{e}_2$ denotes the polarization-direction of the probe pulse.

The differential absorption spectra for resonant excitation at the exciton resonance with co-circular polarized pump and probe pulses, *i.e.* $\mathbf{e}_1 = \mathbf{e}_2 = \boldsymbol{\sigma}^+$, using a pump pulse with $\bar{t}_1 = 1$ ps for different pump-probe time delays are shown in Figures 2a, c, and e (note that the zero of the energy scale is chosen to coincide with the energy of the 1s-exciton). The spectral width of the pump-pulse is much narrower than the exciton binding energy of 15.1 meV. For the probe pulse $\bar{t}_2 = 10$ fs has been used, corresponding to a spectrally flat probe spectrum in the frequency region of interest. For excitation with $\mathbf{e}_1 = \mathbf{e}_2 = \boldsymbol{\sigma}^+$ also $\delta\mathbf{P}(t,\tau)$ has the same polarization as the pulses. Figure 2a shows $\delta\alpha(\omega)$ for a positive delay of $\tau = 2$ ps. The differential absorption is strictly negative in the vicinity of the exciton resonance corresponding to a pump-pulse-induced bleaching of the exciton resonance. The positive contributions to $\delta\alpha(\omega)$ are related to excited state absorption induced by two-exciton states. For energies larger than the exciton energy we see in Figure 2a two positive peaks indicating some structure in the two-exciton continuum.

The total differential absorption can be written as the sum of three contributions (see discussion following Eq. (10) and Appendix A)

$$\delta\alpha(\omega,\tau) = \delta\alpha_{pb}(\omega,\tau) + \delta\alpha_{\mathrm{CI,1st}}(\omega,\tau) + \delta\alpha_{\mathrm{CI,corr}}(\omega,\tau). \quad (19)$$

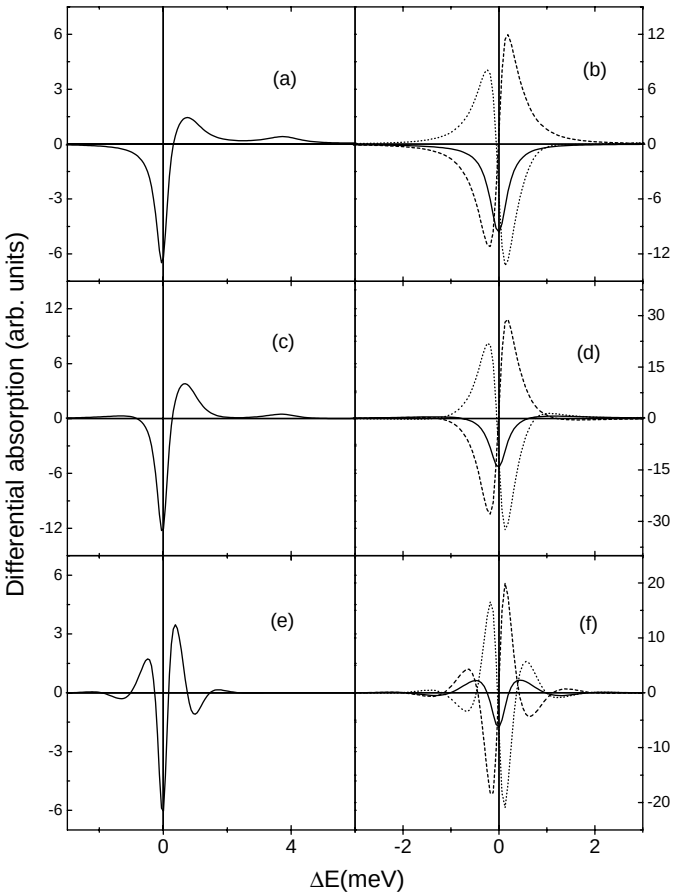

Fig. 2. Differential absorption spectra for resonant excitation at the exciton resonance with co-circular polarized pump ($\boldsymbol{\sigma}^+$) and probe ($\boldsymbol{\sigma}^+$) pulses for different time delays. $\delta\alpha$ is displayed in (a) for $\tau = 2$ ps, (c) $\tau = 0$ ps, and (e) $\tau = -2$ ps. (b), (d), and (f) shows the three contributions to $\delta\alpha$: $\delta\alpha_{pb}$ multiplied by 5 (solid), $\delta\alpha_{\mathrm{CI,1st}}$ (dashed), and $\delta\alpha_{\mathrm{CI,corr}}$ (dotted). Here and in all following figures the 1s-exciton energy coincides with the zero of the energy scale.

Here pb denotes the optical nonlinearity induced by Pauli-blocking. The terms denoted with CI are due to Coulomb-interaction-induced nonlinearities. CI,1st is the first-order (Hartree-Fock) term, and CI,corr the higher-order correlation contribution. These three contributions are displayed separately in Figure 2b. It is shown that $\delta\alpha_{pb}$ is weak (note that it is multiplied by 5 in Fig. 2b) and corresponds to a bleaching at the exciton resonance. $\delta\alpha_{\mathrm{CI,1st}}$ is very strong and is antisymmetric around the exciton resonance (*cp.* Eq. (A.17)). Its dispersive shape corresponds to a blue shift of the exciton. $\delta\alpha_{\mathrm{CI,corr}}$ is also mainly dispersive around the exciton resonance, but with opposite sign compared to $\delta\alpha_{\mathrm{CI,1st}}$, *i.e.* this term yields a red shift. Besides contributions with resonances at the exciton energy, $\delta\alpha_{\mathrm{CI,corr}}$ also includes terms having resonances at the energies of unbound two-exciton states (see Eq. (A.18)). Therefore it is not completely antisymmetric around the exciton resonance. When adding up these three contributions to obtain the total signal *via* equation (19), strong cancellations occur between $\delta\alpha_{\mathrm{CI,1st}}$ and $\delta\alpha_{\mathrm{CI,corr}}$ and the resulting differential absorption (Fig. 2a) shows a predominantly absorptive spectral shape around the exciton resonance. As already indicated earlier when comparing equations (10, 11) and equations (14, 15) (see also analytical results in Appendix A), part of $\delta\alpha_{\mathrm{CI,corr}}$ compensates the first-order term $\delta\alpha_{\mathrm{CI,1st}}$. Additionally $\delta\alpha_{\mathrm{CI,corr}}$ induces some real *correlation*-contributions due to the presence of two-exciton resonances and additionally participates in the bleaching at the exciton (see Eq. (A.18)). In fact, the bleaching at the exciton resonance in Figure 2a is dominated by $\delta\alpha_{\mathrm{CI,corr}}$ and only weakly enhanced by $\delta\alpha_{pb}$.

For $\tau = 0$, Figures 2c and d, we find differential absorption spectra that are qualitatively similar as those at $\tau = 2$ ps. The main differences can be attributed to weak positive contributions for energies below the exciton energy. These are related to the coherent oscillations, which become very prominent for negative pump-probe delays [36]. For $\tau = -2$ ps, see Figure 2e, coherent oscillations dominate the differential absorption spectra. Figure 2f shows that they are present in all three contributions. All of these numerical results can be analyzed qualitatively on the basis of the analytical model results presented in Appendix A.

We now consider excitation with oppositely circularly polarized pulses $\mathbf{e}_1 = \boldsymbol{\sigma}^+$ and $\mathbf{e}_2 = \boldsymbol{\sigma}^-$. For this polarization geometry $\delta\alpha_{pb}$ vanishes, and also $\delta\alpha_{\mathrm{CI,1st}}$ vanishes as long as the system is homogeneous. This is due to the fact that none of these contributions introduces any coupling between the subspaces of different spin states. Therefore, for this polarization geometry, the total signal is identical to the correlation contribution, $\delta\mathbf{P} = \delta\mathbf{P}|_{\mathrm{CI,corr}}$. Using equation (A.11) it can be easily shown that $\delta\mathbf{P}|_{\mathrm{CI,corr}}$ is $\boldsymbol{\sigma}^-$ polarized as the probe pulse. We obtain the spectra displayed by the solid lines in Figures 3a, c, and e. For positive and zero delay (Figs. 3a and c) we again find (negative) bleaching at the exciton and (positive) excited-state absorption due to transitions to two-exciton states. Whereas for co-circular polarized excitation only contributions from unbound two-exciton states are present, now there is a clear signature of a bound biexciton in the differential absorption spectra, appearing about 2.7 meV below the excitonic resonance. For negative delay, see Figure 3e, also in this case coherent oscillations appear. Again, these numerical results can be understood on the basis of the analytical results presented in Appendix A.

We now discuss the influence of detuning of the pump pulse below the exciton resonance for co-circular polarized excitation. Figure 4 shows the resulting differential absorption spectra for various detunings of -1.51 meV, -3.02 meV, -7.5 meV, and -22.6 meV of the pump-pulse energy below the exciton energy. The higher detunings (-7.5 meV and -22.6 meV) are much larger than both the spectral width of the pump pulse and the homogeneous width of the exciton resonance The solid line gives the full $\delta\alpha$, whereas the dashed line gives the result within the time-dependent Hartree-Fock approximation where correlations are neglected, *i.e.* $\delta\alpha_{\mathrm{HF}} = \delta\alpha_{pb} + \delta\alpha_{\mathrm{CI,1st}}$. With increasing detuning the bleaching at the exciton resonance develops into a dispersive shape

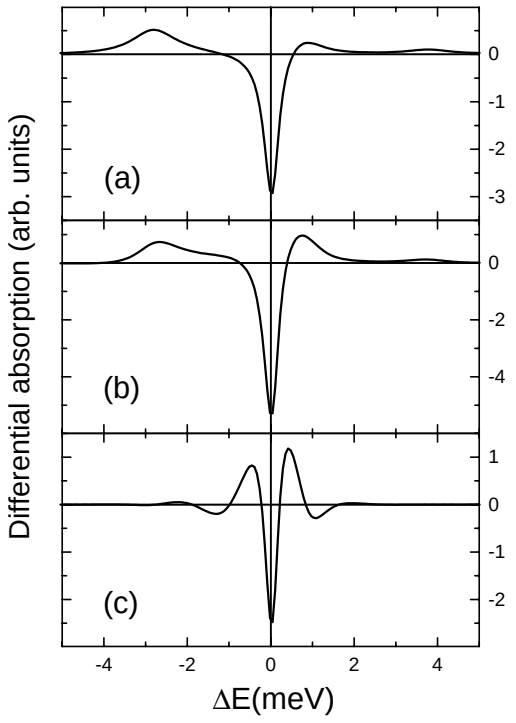

Fig. 3. Differential absorption spectra for resonant excitation at the exciton resonance with opposite circular polarized pump ($\boldsymbol{\sigma}^+$) and probe ($\boldsymbol{\sigma}^-$) pulses for different time delays. $\delta\alpha$ is displayed in (a) for $\tau = 2$ ps, (b) $\tau = 0$ ps, and (c) $\tau = -2$ ps.

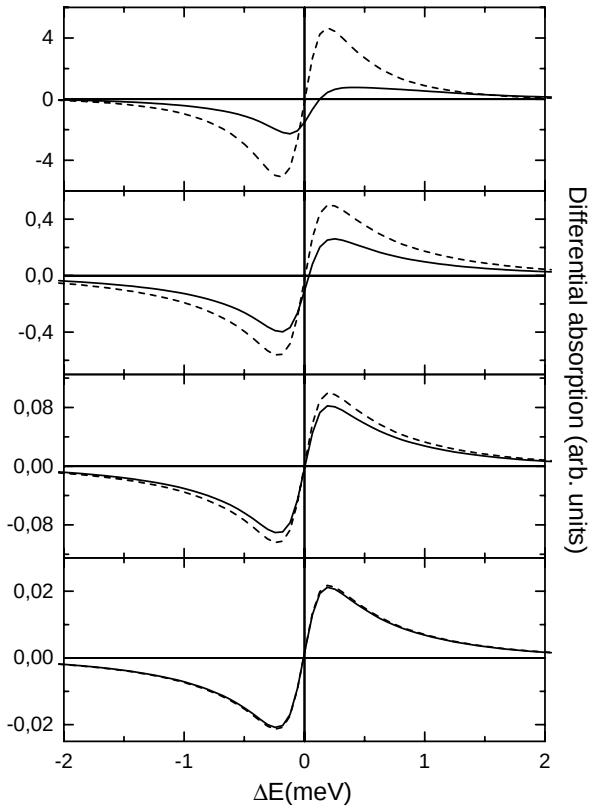

Fig. 4. Differential absorption spectra for various detunings of the pump pulse below the exciton resonance with co-circular polarized pump and probe pulses for zero time-delay. The central frequency of the pump pulse is chosen (a) −1.51 meV, (b) −3.02 meV, (c) −7.5 meV, and (d) −22.6 meV below the energy of the 1*s*-exciton. The solid line gives the full $\delta\alpha$, and the dashed line the result of a Hartree-Fock calculation ($\delta\alpha_{pb} + \delta\alpha_{\mathrm{CI,1st}}$) neglecting correlations ($\delta\alpha_{\mathrm{CI,corr}}$).

corresponding to a blue-shift [36]. Furthermore it is shown in Figure 4 that the importance of the carrier-correlations diminishes rapidly with increasing detuning. We thus conclude that the time-dependent Hartree-Fock approximation gives a good description for this polarization-configuration as long as off-resonant excitation is considered.

5 Numerical results including energetic disorder

Now we discuss results for our model system where we additionally include disorder effects. We implement spatial energetic disorder by assuming a Gaussian distribution of the electron site energy ϵ_c, while the hole energies ϵ_v remain unchanged, *i.e.* ordered. To achieve sufficient convergence, the numerical results are averaged over 120 realizations for a disorder of 2.35 meV (full width at half maximum of the Gaussian distribution) and over 180 realizations for a disorder of 4.70 meV, respectively.

Figure 5 shows the numerical results considering excitation at the energetic position of the disorder-free exciton. First the results for co-circular polarized exciting pulses are discussed. Figure 5a displays $\delta\alpha$ for $\tau = -2$ ps without disorder (solid), with a disorder of 2.35 meV (dashed), and with a twice as strong disorder (dotted). It is shown that the amplitudes of the coherent oscillations which dominate the signal of the perfect sample are strongly reduced with increasing disorder. This can be simply understood by the fact that the disorder partially acts as an inhomogeneous broadening. If the coherent oscillations are averaged over an inhomogeneous distribution with a width comparable to or larger than the energetic period of the coherent oscillations, the resulting $\delta\alpha$ becomes much smaller. Figure 5c displays $\delta\alpha$ for $\tau = 2$ ps. One can identify that the disorder induces the expected red-shift of the maximum of the bleaching as well as some broadening of the exciton line. Furthermore, the two-peak structure in the excited-state absorption present for the ordered case, is averaged out with increasing disorder. The general lineshape of $\delta\alpha$ for excitation with co-circular polarized pulses, *i.e.* a bleaching at the exciton resonance and excited state absorption for higher energies induced by unbound two-exciton states, however, survives even in the presence of disorder. The three contributions to $\delta\alpha$ for $\tau = 2$ ps and strong disorder are displayed separately in Figure 5e. As in the ordered case both $\delta\alpha_{\mathrm{CI,1st}}$ and $\delta\alpha_{\mathrm{CI,corr}}$ are quite large and strongly cancel each other. Compared to the ordered case $\delta\alpha_{pb}$ becomes relatively

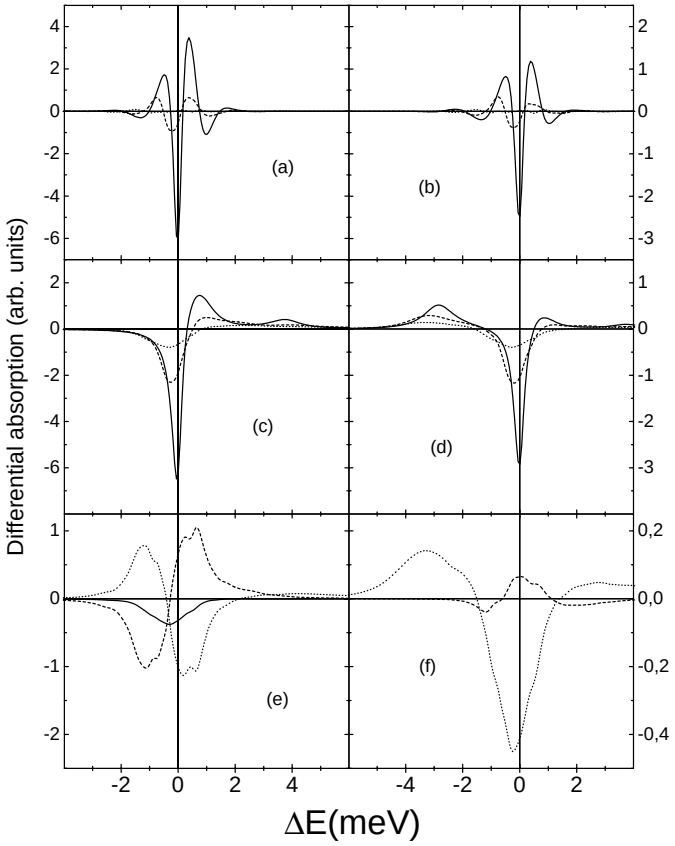

Fig. 5. Differential absorption spectra for resonant excitation at the exciton resonance. (a) co-circular polarized pump and probe pulses and $\tau = -2$ ps, solid: ordered system, dashed: 2.35 meV (FWHM) Gaussian disorder, dotted: 4.70 meV Gaussian disorder. (b) same as (a) for opposite circular polarized pump and probe pulses. (c) same as (a) for $\tau = 2$ ps. (d) same as (b) for $\tau = 2$ ps. (e) shows the three contributions to $\delta\alpha$ displayed in (c): $\delta\alpha_{pb}$ (solid), $\delta\alpha_{\mathrm{CI,1st}}$ (dashed), and $\delta\alpha_{\mathrm{CI,corr}}$ (dotted). (f) shows the two contributions to $\delta\alpha$ displayed in (d): $\delta\alpha_{\mathrm{CI,1st}}$ (dashed), and $\delta\alpha_{\mathrm{CI,corr}}$ (dotted).

larger, and for these present parameters is responsible for about half of the bleaching at the exciton resonance.

Next, we discuss the results obtained for oppositely circularly polarized pump-probe pulses. Figure 5b displays $\delta\alpha$ for $\tau = -2$ ps without disorder (solid), with a disorder of 2.35 meV (dashed), and with a twice as strong disorder (dotted). As in Figure 5a, also Figure 5b shows that the coherent oscillations are strongly suppressed by the disorder. Figure 5d displays $\delta\alpha$ for $\tau = 2$ ps. As in Figure 5c, one can identify that the disorder induces the expected red-shift of the maximum of the bleaching as well as some broadening of the exciton line. Also the positive low-energy biexciton peak, which in the ordered case appears 2.7 meV below the excitonic resonance, shifts towards lower energies and is broadened. The energetic shift of the biexciton line is approximately twice as large as the shift of the exciton. Even for the strongest disorder of 4.70 meV considered here, which is larger than the biexciton binding energy, there is still a pronounced biexciton peak present in $\delta\alpha$. This is consistent with time-integrated four-wave-mixing experiments [12], which reported pronounced exciton-biexciton beats in extremely strong disordered quantum-well samples.

It can thus be concluded, that for the model and parameters investigated here, the disorder, besides some red-shifting of both the exciton as well as the biexciton contributions, mainly induces a correlated inhomogeneous broadening of the one- and two-exciton states. The two contributions (for the present case of disorder plus excitation with oppositely circularly polarized pulses we have $\delta\alpha = \delta\alpha_{\mathrm{CI,1st}} + \delta\alpha_{\mathrm{CI,corr}}$, since $\delta\alpha_{pb}$ vanishes) to $\delta\alpha$ for $\tau = 2$ ps and strong disorder are displayed separately in Figure 5f. The first-order Coulomb contribution which vanishes in the ordered case, becomes finite with disorder. Compared to the correlation contribution it is, however, quite small.

6 Numerical results for a homogeneous system placed inside a microcavity

The microcavity system consists of two distributed Bragg mirrors with alternating GaAs/AlAs $\frac{\lambda}{4}$-layers (index of refraction $n = 3.61$ and $n = 2.95$, respectively) on a GaAs-substrate. The $\frac{3}{2}\lambda$ spacing between the mirrors leads to two anti-nodes inside the cavity [37]. The semiconductor material, that resonantly interacts with the cavity field, is placed at one of these anti-nodes where it is supposed to be excited homogeneously. The frequency of the cavity mode is chosen to coincide with the 1s-exciton resonance of the system. The strong coupling between the cavity mode and the exciton leads to the so-called normal-mode splitting [23].

The propagation of the pulses along the cavity is modeled as in reference [24] using the transfer matrix technique. The pump-probe signal is calculated for resonant excitation where the pump frequency is equal to the free-cavity and free-exciton frequencies assuming zero delay $\tau = 0$ between the pulses. We separately determine the propagation of the fields in $\mathbf{k}_1$ (pump) direction, as well as first- and third-order components of the field in $\mathbf{k}_2$ (probe) direction. In the spectrum of the frequency-domain reflected field $\mathbf{E}_R(\omega)$ in probe-direction $\mathbf{k}_2$ we distinguish between linear and third-order nonlinear contributions,

$$\mathbf{E}_R(\omega) = \mathbf{E}_R^{(1)}(\omega) + a\mathbf{E}_R^{(3)}(\omega), \tag{20}$$

where a depends on the intensity of the pump pulse and is chosen such that the third-order field $a\mathbf{E}_R^{(3)}(\omega)$ causes only a *small* change of the linear field $\mathbf{E}_R^{(1)}(\omega)$. To determine the strength of the third-order term, one can compare the total intensity $|\mathbf{E}_R(\omega)|^2$ at the normal-mode peaks with the first order contribution $|\mathbf{E}_R^{(1)}(\omega)|^2$. The reflection $R(\omega) = |\mathbf{E}_R(\omega)|^2/|\mathbf{E}_0(\omega)|^2$ is normalized with respect to the spectrum of the applied probe field and the differential reflection $\delta R(\omega)$ is given by the difference of the total

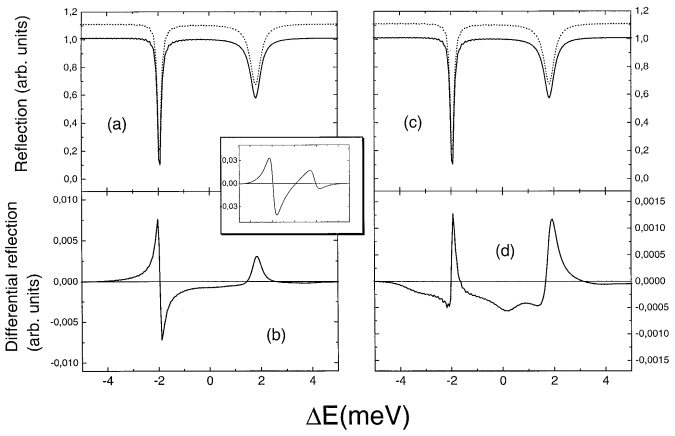

Fig. 6. (a) Probe-reflection $R(\omega)$ (solid) and linear probe-reflection $R^{(1)}(\omega)$ (dotted) for excitation with co-circularly polarized pump and probe pulse and $\tau = 0$ ps. Note that $R^{(1)}(\omega)$ is shifted by 0.1. (b) Resulting differential reflection $\delta R(\omega)$ (Inset: calculation of the differential reflection without correlations, *i.e.* in Hartree-Fock approximation, using the same horizontal scale). (c) and (d) shows the same as (a) and (b) for cross-circularly polarized pump and probe pulses and $\tau = 0$ ps.

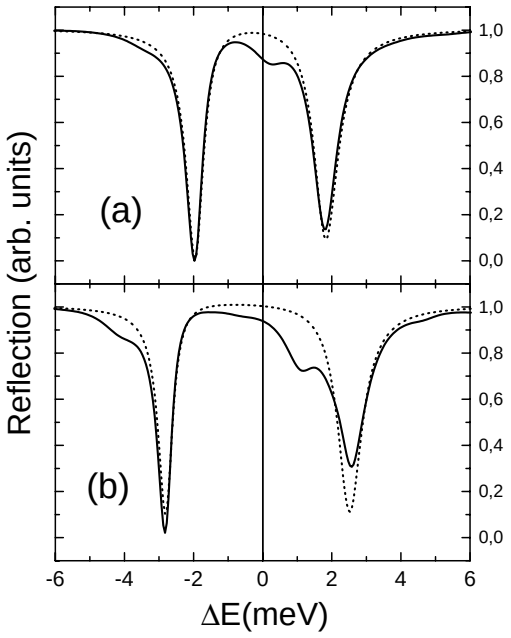

Fig. 7. Total probe-reflection $R(\omega)$ (solid) and linear probe-reflection $R^{(1)}(\omega)$ (dotted) using cross-circularly polarized pump and probe pulses and $\tau = 0$ ps. Two different normal-mode splittings of about 4 meV in (a) and 6 meV (b) are considered.

reflection and the linear reflection,

$$\delta R(\omega) = \frac{|\mathbf{E}_R(\omega)|^2 - |\mathbf{E}_R^{(1)}(\omega)|^2}{|\mathbf{E}_0(\omega)|^2} \,. \tag{21}$$

Taking the third-order field amplitude to be much smaller than the first-order one and assuming a short, *i.e.* spectrally broad, probe pulse results in

$$\delta R(\omega) \propto \mathrm{Re}\left[\mathbf{E}_R^{(1)}(\omega)^* \mathbf{E}_R^{(3)}(\omega)\right] . \tag{22}$$

For our numerical analysis, we use 14 and 16.5 mirror layer pairs for the top and bottom mirror, respectively. In this section the electronic parameters of the semiconductor model system are modified ($U_0 = 8$ meV, $J_c = 8$ meV and $J_v = 0.8$ meV, *i.e.* the energetic parameters are simply multiplied by 8/15 compared to the two previous sections). The resulting reduced exciton binding energy of $E_X = 8.0$ meV is similar to that of the experimental system studied in reference [27]. With these parameters the biexciton binding energy E_{BX} is about 1.4 meV.

The LHS of Figure 6 shows the microcavity reflectivity spectrum for co-circular ($\sigma^+\sigma^+$) excitation with a temporal width of the pump pulse $\bar{t}_1 = 1$ ps. In Figure 6a, the reflections with and without pump are compared, showing that the effect of the third-order contributions is small so that the $\chi^{(3)}$ treatment is valid. Note that the spectra have been shifted with respect to each other in order to show the dashed lines. Figure 6b displays the resulting differential reflection $\delta R(\omega)$. While the energetically higher normal-mode peak exhibits bleaching, the lower peak shifts blue, giving rise to an overall *decrease* of the normal-mode splitting. The inset shows that this shift remains when the calculation is performed without correlations, *i.e.*, in Hartree-Fock approximation. In this approximation, however, also the bleaching of the upper peak becomes a blue shift as well. This demonstrates that also inside a microcavity the correlation effects exhibit characteristic signatures. In Figures 6c and d we show the results for cross-circular ($\sigma^+\sigma^-$) excitation. Note that also within the cavity, for this choice of polarizations the signal is solely due to correlations. Again, we find bleaching of the upper, and a dispersive shape at the lower resonance; this time, however, corresponding to a red shift and therefore an *increase* of the normal-mode splitting. Qualitatively, these results agree well with the experimental findings of Fan *et al.* [27], which were performed on quantum-wells. For the cross-circular polarization we find additional structure in the differential reflection spectra, presented in Figure 6d, which are analyzed in the following.

In order to be able to more clearly investigate the peak structure appearing for cross-circular polarization the parameters are modified as follows: The reflectivity of the mirrors is reduced by changing the number of top and bottom layer pairs to 10 and 12.5, respectively. Furthermore, the dephasing times are doubled ($\gamma_p^{-1} = 6$ ps and $\gamma_B^{-1} = 3$ ps) and, finally, excitation with a short pump pulse ($\bar{t}_1 = 100$ fs) is assumed.

In Figure 7, full reflection spectra (solid) for $\sigma^+\sigma^-$-excitation are shown in comparison to the linear spectra (dashed) (note that in Fig. 7 the same constant a is used as in Fig. 6). In Figure 7a, the normal-mode

splitting was taken to be the same as in Figure 6, while in (b) it has been enhanced by enlarging the dipole matrix element μ_0. The peak in between the normal-mode resonances, which is also present in Figure 6d, is somewhat stronger for the present parameters. Furthermore, in Figures 7a and b a similar shoulder can be seen below the lower normal-mode resonance. In Figures 7a and b the energetic distance of these peaks to the normal-mode resonances coincides with the biexciton binding energy. This appearance of biexcitons in the reflection spectra is to be expected on the basis of our model. Since the field inside the cavity is in resonance with the exciton their coupling leads to the normal-mode splitting giving rise to two resonances. The two-exciton states, however, are not directly coupled to the cavity field and thus remain unchanged inside the cavity (no biexciton normal-mode coupling exists). Therefore, the biexciton should show up one biexciton binding energy below both normal-mode-coupled resonances, as is shown in Figures 7a and b. Another feature that can be seen in Figure 7b is connected to the intensity of the peaks. Whereas the dip in the reflection at the lower normal-mode resonance is stronger than at the upper normal-mode resonance, the intensity of the biexciton-induced features appearing below these resonances behave oppositely. This can be rationalized as follows: the normal-mode splitting is about four times larger than the biexciton binding energy, therefore the frequency difference between the *upper* normal-mode resonance and the biexciton is close to the frequency of the *lower* resonance, and *vice versa*. Thus, when the pump excites the upper normal-mode resonance, a probe frequency close to the lower resonance is needed in order to spectrally excite the biexciton. This explains the obvious *reversal* of the intensities of the biexciton-induced peaks, seen in Figure 7b.

7 Summary

A theoretical analysis of the influence of carrier correlations and disorder on excitonic differential absorption spectra is presented. Numerical results within the coherent $\chi^{(3)}$-limit are obtained for a one-dimensional model allowing us to fully include Coulomb-induced carrier-correlations and to treat bound and unbound two-exciton states on equal footing. For resonant excitation at the exciton resonance we find significant modifications due to the Coulomb correlations. For resonant excitation with co-circularly polarized pulses part of the correlation contributions are shown to cancel first-order Coulomb contributions. The resulting differential absorption spectra show for positive delays bleaching of the exciton and excited-state absorption induced by unbound two-excitons. For negative delays the differential absorption spectra are dominated by the well-known coherent oscillations. When the pump pulse is detuned below the exciton resonance, the correlations are shown to become unimportant for co-circularly polarized pulses. For excitation with opposite circularly polarized pump and probe pulses the differential absorption is solely due to the Coulomb-correlations

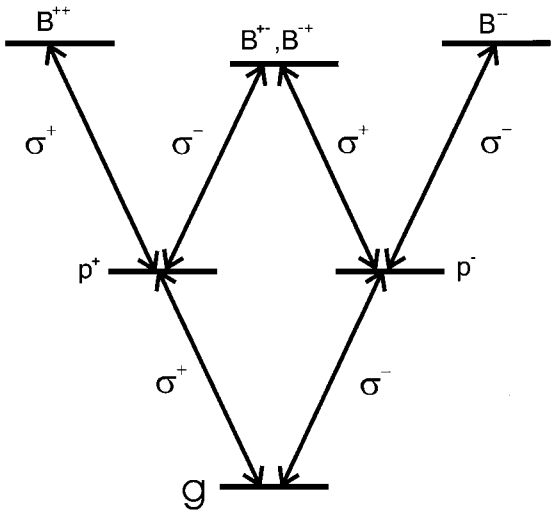

Fig. 8. Schematical drawing of the reduced system considered in Appendix A.

which lead to a coupling between the subspaces of different spin states. In the differential spectra we find positive signatures from both bound (biexciton) and unbound two-exciton states, as well as bleaching signatures at the excitonic resonance for positive delays. For negative delays again coherent oscillations appear.

With energetic disorder the coherent oscillations for negative delays are strongly reduced in amplitude. For positive delays with disorder the bleaching peak at the exciton resonance red shifts and broadens. The biexcitonic excited state absorption peak below the exciton resonance red shifts about twice as much as the excitonic resonance and also broadens. The two-peak structure of the excited state absorption which indicates structure in the continuum of two-exciton states vanishes due to the disorder-induced broadening.

When the excitonic system is placed inside a microcavity we find a strong polarization dependence of the differential reflection signal. The calculated signatures appearing at the upper and lower exciton-cavity modes are in good agreement with recent experiments [27]. Additionally, our calculations reveal further correlation-induced contributions, representing additional resonances associated with excitation of the biexciton, in the differential reflection which should be observable in high-quality samples.

This work is supported by the Deutsche Forschungsgemeinschaft through the Sonderforschungsbereich 383, the Heisenberg program (F.J.), and the Leibniz Prize (S.W.K.). We acknowledge the John von Neumann Institut für Computing (NIC), Forschungszentrum Jülich, Germany, for extended CPU time on their supercomputer systems. S.W.K. and F.J. thank J. Moloney, ACMS, University of Arizona, for hospitality during the final part of this work.

Appendix A: Analytical results for simplified model

In this Appendix we project the full equations for p^{11}, p^{22}, B^{1111}, B^{2222}, and B^{1122} onto the respective single relevant states, as is shown schematically in Figure 8. For p^{11} this state is called p^+, which is the $1s$ exciton that can be excited with $\boldsymbol{\sigma}^+$ polarized light. Similarly, we project p^{22} onto p^-, which can be excited with $\boldsymbol{\sigma}^-$ polarized light. Both p^+ and p^- refer to the $1s$ exciton and have the same frequency ϵ_x.

A similar projection onto B^{++} and B^{--} for B^{1111} and B^{2222} is performed. As pointed out above, for excitation with two co-circularly polarized pulses typically no bound biexcitons are excited, therefore B^{++} and B^{--} represent in this case unbound two-exciton states with frequencies $\epsilon_{2x} > 2\epsilon_x$. For B^{1122} we introduce B^{+-} to represent a biexciton with frequency $\epsilon_{bx} < 2\epsilon_x$.

The simplified level scheme given by Figure 8 is different to the one used in reference [9]. First, instead of just the biexciton also unbound two-exciton states (B^{1111} and B^{2222}) are included. Second, within the microscopic density matrix theory the interband polarization $\mathbf{P}$ is determined purely by the interband coherence p, whereas in reference [9] also the transitions from the excitons to the biexciton contributed to the polarization. Instead of using density matrix theory the scheme used in reference [9] corresponds to expressing the optical response using the many-body eigenstates of the system. Within this picture the optical response is expressed using the energies and transitions between the many-body eigenstates [38].

Projecting equations (10, 11) onto the states described above results in the following equations of motion (see also Ref. [3] where similar equations have been derived [39])

$$\begin{aligned} -\mathrm{i}\partial_t p^+ = &-(\epsilon_x - \mathrm{i}\gamma_x)p^+ + \mathbf{E}\cdot(\boldsymbol{\sigma}^+)^*(\phi(0)^* - 2b|p^+|^2) \\ &- V(p^+|p^+|^2) + \tilde{V}(p^+|p^-|^2) \\ &- V_B B^{+-}(p^-)^* + \tilde{V}_B B^{++}(p^+)^*, \end{aligned} \tag{A.1}$$

$$\begin{aligned} -\mathrm{i}\partial_t p^- = &-(\epsilon_x - \mathrm{i}\gamma_x)p^- + \mathbf{E}\cdot(\boldsymbol{\sigma}^-)^*(\phi(0)^* - 2b|p^-|^2) \\ &- V(p^-|p^-|^2) + \tilde{V}(p^-|p^+|^2) \\ &- V_B B^{+-}(p^+)^* + \tilde{V}_B B^{--}(p^-)^*, \end{aligned} \tag{A.2}$$

$$-\mathrm{i}\partial_t B^{++} = -(\epsilon_{2x} - \mathrm{i}\gamma_{2x})B^{++} + p^+p^+, \tag{A.3}$$

$$-\mathrm{i}\partial_t B^{--} = -(\epsilon_{2x} - \mathrm{i}\gamma_{2x})B^{--} + p^-p^-, \tag{A.4}$$

and

$$-\mathrm{i}\partial_t B^{+-} = -(\epsilon_{bx} - \mathrm{i}\gamma_{bx})B^{+-} + p^+p^-. \tag{A.5}$$

A number of quantities has been defined in equations (A.1–A.5): $\phi(0)$ is the value of the exciton wavefunction at the origin which describes the excitonic enhancement of the optical transition [29]. Phenomenological dephasing rates γ have been introduced. Since B refers to the correlated part of a general four-point quantity, where uncorrelated contributions proportional to p^2 have been removed, one should use $\gamma_{2x} = \gamma_{bx} = 2\gamma_x$ to be consistent. The quantities b, V, $\tilde{V}$, V_B, and $\tilde{V}_B$ are the optical nonlinearities. b denotes the Pauli-blocking [3,35,40]. V represents the Coulomb interaction between excitons with the same spin [3,35,40]. $\tilde{V}$ is similar but describes the interaction between excitons with opposite spin, which vanishes in a homogeneous system. V_B is the nonlinearity related to the Coulomb-induced coupling between excitons and the biexciton [3], and $\tilde{V}_B$ is the corresponding quantity related to an unbound two-exciton state. V and $\tilde{V}$ are of first-order in the Coulomb interaction, whereas the contributions V_B and $\tilde{V}_B$ are of higher-order. Expressions for these parameters can be obtained simply by explicitly performing the projections of the equations (10, 11) onto the considered single- and two-exciton states [3,35].

Within the simplified model the total polarization $\mathbf{P}$ is given by

$$\mathbf{P} = \phi(0)(\boldsymbol{\sigma}^+p^+ + \boldsymbol{\sigma}^-p^-). \tag{A.6}$$

In the following we summarize our analytical results obtained for the time-domain signal in differential absorption geometry. For this purpose we calculate all contributions to $\delta\mathbf{P}$, *i.e.* to p^+ and p^-, which propagate in the direction the probe pulse ($\mathbf{E}_2$), and which include two interactions with the pump pulse ($\mathbf{E}_1$) and are linear in the probe pulse. We assume δ-pulse excitation

$$\begin{aligned} \mathbf{E}(t) = &\,\delta(t+\tau)(\mathbf{e}_1\mathrm{e}^{\mathrm{i}\mathbf{k_1}\cdot\mathbf{r}} + (\mathbf{e}_1)^*\mathrm{e}^{-\mathrm{i}\mathbf{k_1}\cdot\mathbf{r}}) \\ &+\delta(t)(\mathbf{e}_2\mathrm{e}^{\mathrm{i}\mathbf{k_2}\cdot\mathbf{r}} + (\mathbf{e}_2)^*\mathrm{e}^{-\mathrm{i}\mathbf{k_2}\cdot\mathbf{r}}), \end{aligned} \tag{A.7}$$

where a positive time delay τ corresponds to the pump pulse arriving before the probe pulse.

The total differential polarization $\delta\mathbf{P}(t,\tau)$ can be written as a sum of three terms originating from different optical nonlinearities

$$\delta\mathbf{P}(t,\tau) = \delta\mathbf{P}_{pb}(t,\tau) + \delta\mathbf{P}_{\mathrm{CI,1st}}(t,\tau) + \delta\mathbf{P}_{\mathrm{CI,corr}}(t,\tau). \tag{A.8}$$

Here pb denotes the Pauli-blocking and CI refers to the Coulomb-induced optical nonlinearities which appear in first order within time-dependent Hartree-Fock approximation (CI,1st) and in higher-order due to correlation-induced contributions (CI,corr). Introducing abbreviations for the appearing scalar products between the pulse directions $\mathbf{e}_1$ and $\mathbf{e}_2$ and the transition dipoles $\boldsymbol{\sigma}^+$ and $\boldsymbol{\sigma}^-$ by defining $e_i^+ = \mathbf{e}_i\cdot\boldsymbol{\sigma}^+$ and $e_i^- = \mathbf{e}_i\cdot\boldsymbol{\sigma}^-$, the three terms contributing to the pump-probe signal are

$$\delta\mathbf{P}_{pb}(t,\tau) = -2\mathrm{i}b|\phi(0)|^2[\boldsymbol{\sigma}^+e_1^-(e_1^-)^*e_2^- + \boldsymbol{\sigma}^-e_1^+(e_1^+)^*e_2^+] \times\left(\Theta(\tau)\Theta(t)\mathrm{e}^{-2\gamma_x\tau}\mathrm{e}^{(-\mathrm{i}\epsilon_x-\gamma_x)t} + \Theta(-\tau)\Theta(t+\tau)\mathrm{e}^{(-\mathrm{i}\epsilon_x-\gamma_x)t}\right). \tag{A.9}$$

$$\delta\mathbf{P}_{\mathrm{CI,1st}}(t,\tau) = |\phi(0)|^2\phi(0)^*\left(V[\boldsymbol{\sigma}^+e_1^-(e_1^-)^*e_2^- + \boldsymbol{\sigma}^-e_1^+(e_1^+)^*e_2^+] - \tilde{V}[\boldsymbol{\sigma}^+e_1^+(e_1^+)^*e_2^- + \boldsymbol{\sigma}^-e_1^-(e_1^-)^*e_2^+]\right) \times\left(\Theta(\tau)\Theta(t)\mathrm{e}^{-2\gamma_x\tau}\mathrm{e}^{(-\mathrm{i}\epsilon_x-\gamma_x)t}\frac{1-\mathrm{e}^{-2\gamma_x t}}{2\gamma_x} + \Theta(-\tau)\Theta(t+\tau)\mathrm{e}^{(-\mathrm{i}\epsilon_x-\gamma_x)t}\frac{1-\mathrm{e}^{-2\gamma_x(t+\tau)}}{2\gamma_x}\right). \tag{A.10}$$

$$\begin{aligned}\delta\mathbf{P}_{\mathrm{CI,corr}}(t,\tau) = {}& |\phi(0)|^2\phi(0)^*\tilde{V}_B\left[\boldsymbol{\sigma}^+e_1^-(e_1^-)^*e_2^- + \boldsymbol{\sigma}^-e_1^+(e_1^+)^*e_2^+\right]\\ &\times\left(\Theta(\tau)\Theta(t)\frac{\mathrm{e}^{-2\gamma_x\tau}}{\epsilon_{2x}-2\epsilon_x+\mathrm{i}(2\gamma_x-\gamma_{2x})}\mathrm{e}^{(-\mathrm{i}\epsilon_x-\gamma_x)t}\left(-\frac{1-\mathrm{e}^{-2\gamma_x t}}{2\gamma_x}+\mathrm{i}\frac{1-\mathrm{e}^{(\mathrm{i}(2\epsilon_x-\epsilon_{2x})-\gamma_{2x})t}}{((2\epsilon_x-\epsilon_{2x})+\mathrm{i}\gamma_{2x})}\right)\right.\\ &\left.+\Theta(-\tau)\Theta(t+\tau)\frac{1}{\epsilon_{2x}-2\epsilon_x+\mathrm{i}(2\gamma_x-\gamma_{2x})}\mathrm{e}^{(-\mathrm{i}\epsilon_x-\gamma_x)(t+\tau)}\right.\\ &\left.\times\left(-\frac{1-\mathrm{e}^{-2\gamma_x t}}{2\gamma_x}+\mathrm{i}\frac{1-\mathrm{e}^{(\mathrm{i}(2\epsilon_x-\epsilon_{2x})-\gamma_{2x})t+(\mathrm{i}(2\epsilon_x-\epsilon_{2x})-\gamma_{2x})\tau}}{((2\epsilon_x-\epsilon_{2x})+\mathrm{i}\gamma_{2x})}\right)\right)\\ &-|\phi(0)|^2\phi(0)^*V_B\left[\boldsymbol{\sigma}^+(e_1^+)^*[e_1^+e_2^- + e_1^-e_2^+] + \boldsymbol{\sigma}^-(e_1^-)^*[e_1^-e_2^+ + e_1^+e_2^-]\right]\\ &\times\left(\Theta(\tau)\Theta(t)\frac{\mathrm{e}^{-2\gamma_x\tau}}{\epsilon_{bx}-2\epsilon_x+\mathrm{i}(2\gamma_x-\gamma_{bx})}\mathrm{e}^{(-\mathrm{i}\epsilon_x-\gamma_x)t}\left(-\frac{1-\mathrm{e}^{-2\gamma_x t}}{2\gamma_x}+\mathrm{i}\frac{1-\mathrm{e}^{(\mathrm{i}(2\epsilon_x-\epsilon_{bx})-\gamma_{bx})t}}{((2\epsilon_x-\epsilon_{bx})+\mathrm{i}\gamma_{bx})}\right)\right.\\ &\left.+\Theta(-\tau)\Theta(t+\tau)\frac{1}{\epsilon_{bx}-2\epsilon_x+\mathrm{i}(2\gamma_x-\gamma_{bx})}\mathrm{e}^{(-\mathrm{i}\epsilon_x-\gamma_x)(t+\tau)}\right.\\ &\left.\times\left(-\frac{1-\mathrm{e}^{-2\gamma_x t}}{2\gamma_x}+\mathrm{i}\frac{1-\mathrm{e}^{(\mathrm{i}(2\epsilon_x-\epsilon_{bx})-\gamma_{bx})t+(\mathrm{i}(2\epsilon_x-\epsilon_{bx})-\gamma_{bx})\tau}}{((2\epsilon_x-\epsilon_{bx})+\mathrm{i}\gamma_{bx})}\right)\right).\end{aligned} \tag{A.11}$$

given by For positive time-delay $\delta\mathbf{P}_{pb}(t,\tau)$ decays with $\mathrm{e}^{-2\gamma_x\tau}$, since the pump pulse creates two polarizations p and p^* which decay during the time interval τ. The factor $\mathrm{e}^{(-\mathrm{i}\epsilon_x-\gamma_x)t}$ originates from the polarization created by the probe field at $t=0$. Exactly the same terms ($\mathrm{e}^{-2\gamma_x\tau}$ and $\mathrm{e}^{(-\mathrm{i}\epsilon_x-\gamma_x)t}$) appear in the expressions for $\delta\mathbf{P}_{\mathrm{CI,1st}}(t,\tau)$ and $\delta\mathbf{P}_{\mathrm{CI,corr}}(t,\tau)$. In $\delta\mathbf{P}_{pb}$ no mixing between the excitons with different polarizations occurs. The same is true for the term proportional to V in $\delta\mathbf{P}_{\mathrm{CI,1st}}$. Apart from a different complex prefactor (V instead of $-2\mathrm{i}b$) and the rising envelope ($(1-\mathrm{e}^{-2\gamma_x t})/(2\gamma_x)$) this term is identical to the $\delta\mathbf{P}_{pb}$. The time-dependence of the term proportional to $\tilde{V}$ in $\delta\mathbf{P}_{\mathrm{CI,1st}}$ is identical to the term proportional to V, they, however, have different selection rules. $\tilde{V}$ introduces a coupling between the excitons with different polarizations, which may be be finite in an inhomogeneous (for example disordered) system, but vanishes in a homogeneous system.

Classifying the contributions to $\delta\mathbf{P}_{\mathrm{CI,corr}}(t,\tau)$ with respect to the selection rules, the term proportional to $\tilde{V}_B$ introduces no coupling between the excitons with different polarizations, whereas the term proportional to V_B does. Concerning the temporal-evolution, $\delta\mathbf{P}_{\mathrm{CI,corr}}$ includes two types of terms. The first one is, apart from a prefactor $-1/(\epsilon_{xx}-2\epsilon_x+\mathrm{i}(2\gamma_x-\gamma_{xx}))$ (here xx stands for $2x$ or bx), identical to the first-order Coulomb-contribution. This term induces strong cancellations of the first-order contribution. (as is also concluded comparing Eqs. (10, 11) and Eqs. (14, 15)). The second term is proportional to $\mathrm{i}(1-\mathrm{e}^{(\mathrm{i}(2\epsilon_x-\epsilon_{xx})-\gamma_{xx})t})/(((2\epsilon_x-\epsilon_{xx})+\mathrm{i}\gamma_{xx}))$ and introduces the two-exciton energies explicitly into the temporal evolution.

A Fourier-transform of the time-domain results

$$\delta\mathbf{P}(\omega,\tau) = \int \mathrm{d}t\mathrm{e}^{\mathrm{i}\omega t}\delta\mathbf{P}(t,\tau), \tag{A.12}$$

gives the τ dependent frequency-domain differential polarization $\delta\mathbf{P}(\omega,\tau)$. After projecting onto the probe polarization and assuming a spectrally broad probe pulse,

we obtain

$$\delta\chi(\omega,\tau) \propto \mathbf{e}_2^* \cdot \delta\mathbf{P}(\omega,\tau). \tag{A.13}$$

Hence, $\delta\mathbf{P}$ is proportional to the differential susceptibility $\delta\chi$, whose imaginary part determines the differential absorption $\delta\alpha$ [29]

$$\delta\alpha(\omega,\tau) \propto \mathrm{Im}[\delta\chi(\omega,\tau)] \propto \mathrm{Im}[\mathbf{e}_{\mathrm{detect}}^* \cdot \delta\mathbf{P}(\omega,\tau)]. \tag{A.14}$$

Similarly to $\delta\mathbf{P}$, see equation (A.8), $\delta\alpha$ can be written as a sum of three contributions

$$\delta\alpha(t,\tau) = \delta\alpha_{pb}(t,\tau) + \delta\alpha_{\mathrm{CI,1st}}(t,\tau) + \delta\alpha_{\mathrm{CI,corr}}(t,\tau). \tag{A.15}$$

For the analysis of the differential absorption spectra we concentrate on the time-dependent terms contained in equations (A.9–A.11). Furthermore, we assume that the polarization direction of $\delta\mathbf{P}$ is the same as the polarization direction of the probe pulse $\mathbf{e}_2$, which is fulfilled for co- and opposite circular polarized excitation as can easily be verified using equations (A.9–A.11). We start this discussion considering positive τ. For $\delta\alpha_{pb}$ we get

$$\begin{aligned}\delta\alpha(\omega,\tau)|_{pb,\tau>0} \; &\propto \mathrm{Im}[\int_0^\infty \mathrm{d}t - \mathrm{i}\mathrm{e}^{-2\gamma_x\tau}\mathrm{e}^{(-\mathrm{i}(\epsilon_x-\omega)-\gamma_x)t}] \\ &= \mathrm{e}^{-2\gamma_x\tau}\frac{-\gamma_x}{(\epsilon_x-\omega)^2+\gamma_x^2}.\end{aligned} \tag{A.16}$$

This term simply describes a bleaching of the exciton resonance caused by the excitation of the pump pulse [29,36,41]. For the $\delta\alpha_{\mathrm{CI,1st}}$ term we get

$$\begin{aligned}&\delta\alpha(\omega,\tau)|_{\mathrm{CI,1st},\tau>0} \propto \\ &\mathrm{Im}[\int_0^\infty \mathrm{d}t\mathrm{e}^{-2\gamma_x\tau}\mathrm{e}^{(-\mathrm{i}(\epsilon_x-\omega)-\gamma_x)t}\frac{1-\mathrm{e}^{-2\gamma_x t}}{2\gamma_x}] = \\ &\mathrm{e}^{-2\gamma_x\tau}\frac{1}{2\gamma_x}\left(\frac{-(\epsilon_x-\omega)}{(\epsilon_x-\omega)^2+\gamma_x^2} - \frac{-(\epsilon_x-\omega)}{(\epsilon_x-\omega)^2+9\gamma_x^2}\right).\end{aligned} \tag{A.17}$$

This is the well-known blue-shift of the excitonic resonance which in a Hartree-Fock calculation for resonant excitation dominates over the bleaching induced by the Pauli-blocking [29,41,42]. The different spectral shape of $\delta\alpha|_{pb,\tau>0}$ and $\delta\alpha|_{\mathrm{CI,1st},\tau>0}$ originates from the imaginary prefactor $-\mathrm{i}$ contained in $\delta\mathbf{P}_{pb}$ that is not contained in $\delta\mathbf{P}_{\mathrm{CI,1st}}$.

Assuming $2\gamma_x = \gamma_{xx}$ (here xx stands for $2x$ or bx, compare Eq. (A.11)) which makes the prefactor $1/(\epsilon_{xx} - 2\epsilon_x + \mathrm{i}(2\gamma_x - \gamma_{xx}))$ appearing in equation (A.11) real, we get for $\delta\alpha_{\mathrm{CI,corr}}$

$$\begin{aligned}&\delta\alpha(\omega,\tau)|_{\mathrm{CI,corr},\tau>0} \propto \mathrm{Im}\Bigg[-\int_0^\infty \mathrm{d}t\mathrm{e}^{-2\gamma_x\tau}\mathrm{e}^{(-\mathrm{i}(\epsilon_x-\omega)-\gamma_x)t} \\ &\times\left(-\frac{1-\mathrm{e}^{-2\gamma_x t}}{2\gamma_x} - \frac{1-\mathrm{e}^{(\mathrm{i}(2\epsilon_x-\epsilon_{xx})-\gamma_{xx})t}}{(\mathrm{i}(2\epsilon_x-\epsilon_{xx})-\gamma_{xx})}\right)\Bigg] = \mathrm{e}^{-2\gamma_x\tau}\frac{1}{2\gamma_x} \\ &\times\left(-\frac{(\epsilon_x-\omega)}{(\epsilon_x-\omega)^2+\gamma_x^2} - \frac{-(\epsilon_x-\omega)}{(\epsilon_x-\omega)^2+9\gamma_x^2}\right) \\ &-\mathrm{e}^{-2\gamma_x\tau}\left[\frac{1}{((2\epsilon_x-\epsilon_{xx})^2+\gamma_{xx}^2)}\left(\frac{(\omega-\epsilon_x)\gamma_x-(\epsilon_{xx}-2\epsilon_x)\gamma_x}{(\epsilon_x-\omega)^2+\gamma_x^2}\right.\right. \\ &\left.\left.-\frac{(\omega-\epsilon_{xx}+\epsilon_x)\gamma_x-(\epsilon_{xx}-2\epsilon_x)(\gamma_x+\gamma_{xx})}{(\epsilon_{xx}-\epsilon_x-\omega)^2+(\gamma_x+\gamma_{xx})^2}\right)\right].\end{aligned} \tag{A.18}$$

The first two terms of $\delta\alpha_{\mathrm{CI,corr}}$ are just the negative of $\delta\alpha_{\mathrm{CI,1st}}$, which confirms that the first-order terms are canceled by the higher-order correlations, as has been discussed following equations (14, 15). The last two terms of $\delta\alpha_{\mathrm{CI,corr}}$ explicitly include the energies of the two-exciton states. The first one has its resonances at the exciton energy ϵ_x and its spectral shape in the vicinity of ϵ_x corresponds to a bleaching. The last term has its resonances at the difference between the energies of the single-exciton and two-exciton $\epsilon_{xx} - \epsilon_x$ and in the vicinity of $\epsilon_{xx} - \epsilon_x$ has an absorptive shape leading to a positive contribution to $\delta\alpha$. This positive contribution corresponds to induced absorption (or excited-state absorption) due to the presence of single- to two-exciton transitions [43].

We now consider negative τ. For $\delta\alpha_{pb}$ term we get

$$\begin{aligned}&\delta\alpha(\omega,\tau)|_{pb,\tau<0} \propto \mathrm{Im}[\int_{-\tau}^\infty \mathrm{d}t - \mathrm{i}\mathrm{e}^{(-\mathrm{i}(\epsilon_x-\omega)-\gamma_x)t}] = \\ &\mathrm{e}^{-\gamma_x|\tau|}\frac{-\gamma_x\cos((\epsilon_x-\omega)\tau) - (\epsilon_x-\omega)\sin((\epsilon_x-\omega)\tau)}{(\epsilon_x-\omega)^2+\gamma_x^2}.\end{aligned} \tag{A.19}$$

As function of $|\tau|$ $\delta\alpha_{pb}$ decays with γ_x, because the polarization induced by the probe pulse (which comes first for $\tau < 0$) decays during the time period $|\tau|$ before the pump pulse is incident on the sample. The coherent oscillations present in $\delta\alpha_{pb}$ originate from the scattering of the pump pulse of the grating created by both pump and probe pulses into the probe direction [36]. The period of these oscillations is inversely proportional to $|\tau|$ and develops into the (non-oscillating) bleaching for $|\tau| \to 0$ (see Eq. (A.19)) [36].

The Coulomb-induced contributions are given by

$$\delta\alpha(\omega,\tau)|_{\mathrm{CI,1st},\tau<0} \propto$$
$$\mathrm{Im}\left[\int_{-\tau}^{\infty}\mathrm{d}t\mathrm{e}^{-2\gamma_x\tau}\mathrm{e}^{(-\mathrm{i}(\epsilon_x-\omega)-\gamma_x)t}\frac{1-\mathrm{e}^{-2\gamma_x t}}{2\gamma_x}\right]=\mathrm{e}^{-\gamma_x|\tau|}\frac{1}{2\gamma_x}$$
$$\times\left[\cos((\epsilon_x-\omega)\tau)\left(\frac{-(\epsilon_x-\omega)}{(\epsilon_x-\omega)^2+\gamma_x^2}-\frac{-(\epsilon_x-\omega)}{(\epsilon_x-\omega)^2+9\gamma_x^2}\right)\right.$$
$$\left.+\sin((\epsilon_x-\omega)\tau)\left(\frac{\gamma_x}{(\epsilon_x-\omega)^2+\gamma_x^2}-\frac{3\gamma_x}{(\epsilon_x-\omega)^2+9\gamma_x^2}\right)\right], \quad (A.20)$$

$$\delta\alpha(\omega,\tau)|_{\mathrm{CI,corr},\tau<0} \propto$$
$$\mathrm{Im}\left[-\int_{-\tau}^{\infty}\mathrm{d}t\mathrm{e}^{-2\gamma_x\tau}\mathrm{e}^{(-\mathrm{i}(\epsilon_x-\omega)-\gamma_x)t}\right.$$
$$\left.\times\left(-\frac{1-\mathrm{e}^{-2\gamma_x t}}{2\gamma_x}-\frac{1-\mathrm{e}^{(\mathrm{i}(2\epsilon_x-\epsilon_{xx})-\gamma_{xx})t}}{(\mathrm{i}(2\epsilon_x-\epsilon_{xx})-\gamma_{xx})}\right)\right]=\mathrm{e}^{-\gamma_x|\tau|}\frac{1}{2\gamma_x}$$
$$\times\cos((\epsilon_x-\omega)\tau)\left(\frac{-(\epsilon_x-\omega)}{(\epsilon_x-\omega)^2+\gamma_x^2}-\frac{-(\epsilon_x-\omega)}{(\epsilon_x-\omega)^2+9\gamma_x^2}\right)$$
$$-\mathrm{e}^{-\gamma_x\tau}\cos((\epsilon_x-\omega)\tau)\frac{1}{(2\epsilon_x-\epsilon_{xx})^2+\gamma_{xx}^2}$$
$$\times\left(\frac{-(\epsilon_x-\omega)\gamma_{xx}-(\epsilon_{xx}-2\epsilon_x)\gamma_x}{(\epsilon_x-\omega)^2+\gamma_x^2}\right.$$
$$\left.-\frac{-(\epsilon_{xx}-\epsilon_x-\omega)\gamma_{xx}-(\epsilon_{xx}-2\epsilon_x)(\gamma_x+\gamma_{xx})}{(\epsilon_{xx}-\epsilon_x-\omega)^2+(\gamma_x+\gamma_{xx})^2}\right)$$
$$+\mathrm{e}^{-\gamma_x|\tau|}\frac{1}{2\gamma_x}\sin((\epsilon_x-\omega)\tau)$$
$$\times\left(\frac{\gamma_x}{(\epsilon_x-\omega)^2+\gamma_x^2}-\frac{3\gamma_x}{(\epsilon_x-\omega)^2+9\gamma_x^2}\right)$$
$$-\mathrm{e}^{-\gamma_x\tau}\sin((\epsilon_x-\omega)\tau)\frac{1}{(2\epsilon_x-\epsilon_{xx})^2+\gamma_{xx}^2}$$
$$\times\left(\frac{\gamma_x\gamma_{xx}-(\epsilon_{xx}-2\epsilon_x)(\epsilon_x-\omega)}{(\epsilon_x-\omega)^2+\gamma_x^2}\right.$$
$$\left.-\frac{\gamma_{xx}(\gamma_x+\gamma_{xx})-(\epsilon_{xx}-2\epsilon_x)(\epsilon_{xx}-\epsilon_x-\omega)}{(\epsilon_{xx}-\epsilon_x-\omega)^2+(\gamma_x+\gamma_{xx})^2}\right). \quad (A.21)$$

Also in $\delta\alpha_{\mathrm{CI,1st}}$ and $\delta\alpha_{\mathrm{CI,corr}}$ similar spectral oscillations are present as in $\delta\alpha_{pb}$.

References

1. H. Wang, K.B. Ferrio, D.G. Steel, Y.Z. Hu, R. Binder, S.W. Koch, Phys. Rev. Lett. **71**, 1261 (1993); H. Wang, K.B. Ferrio, D.G. Steel, P.R. Berman, Y.Z. Hu, R. Binder, S.W. Koch, Phys. Rev. A **49**, 1551 (1994); Y.Z. Hu, R. Binder, S.W. Koch, S.T. Cundiff, H. Wang, D.G. Steel, Phys. Rev. B **49**, 14382 (1994).
2. T. Rappen, U.G. Peter, M. Wegener, W. Schäfer, Phys. Rev. B **49**, 10774 (1994).
3. W. Schäfer, D.S. Kim, J. Shah, T.C. Damen, J.E. Cunningham, K.W. Goosen, L.N. Pfeiffer, K. Köhler, Phys. Rev. B **53**, 16429 (1996); P. Kner, S. Bar-Ad, M.V. Marquezini, D.S. Chemla, W. Schäfer, Phys. Rev. Lett. **78**, 1319 (1997); P. Kner, W. Schäfer, R. Lövenich, D.S. Chemla, Phys. Rev. Lett. **81**, 5386 (1998).
4. M. Lindberg, Y.Z. Hu, R. Binder, S.W. Koch, Phys. Rev. B **50**, 18060 (1994).
5. V. M. Axt, K. Victor, A. Stahl, Phys. Rev. B **53**, 7244 (1996).
6. B.F. Feuerbacher, J. Kuhl, K. Ploog, Phys. Rev. B **43**, 2439 (1991).
7. S. Bar-Ad, I. Bar-Joseph, Phys. Rev. Lett. **68**, 349 (1992).
8. D.J. Lovering, R.T. Phillips, G.J. Denton, G.W. Smith, Phys. Rev. Lett. **68**, 1880 (1992).
9. K. Bott, O. Heller, D. Bennhardt, S.T. Cundiff, P. Thomas, E.J. Mayer, G.O. Smith, R. Eccleston, J. Kuhl, K. Ploog, Phys. Rev. B **48**, 17418 (1993).
10. J.-Y. Bigot, A. Daunois, J. Oberle, J.-C. Merle, Phys. Rev. Lett. **71**, 1820 (1993).
11. E.J. Mayer, G.O. Smith, V. Heuckeroth, J. Kuhl, K. Bott, A. Schulze, T. Meier, D. Bennhardt, S.W. Koch, P. Thomas, R. Hey, K. Ploog, Phys. Rev. B **50**, 14730 (1994); E.J. Mayer, G.O. Smith, V. Heuckeroth, J. Kuhl, K. Bott, A. Schulze, T. Meier, S.W. Koch, P. Thomas, R. Hey, K. Ploog, Phys. Rev. B **51**, 10909 (1995); K. Bott, E.J. Mayer, G.O. Smith, V. Heuckeroth, M. Hübner, J. Kuhl, T. Meier, A. Schulze, M. Lindberg, S.W. Koch, P. Thomas, J. Opt. Soc. Am. B **13**, 1026 (1996).
12. T.F. Albrecht, K. Bott, T. Meier, A. Schulze, M. Koch, S.T. Cundiff, J. Feldmann, W. Stolz, P. Thomas, S.W. Koch, E.O. Göbel, Phys. Rev. B **54**, 4436 (1996).
13. Th. Östreich, K. Schönhammer, L.J. Sham, Phys. Rev. Lett. **74**, 4698 (1995).
14. V.M. Axt, A. Stahl, Z. Phys. B **93**, 195 (1994); *ibid*, 205 (1994).
15. Th. Östreich, K. Schönhammer, L.J. Sham, Phys. Rev. Lett. **75**, 2554 (1995).
16. G. Bartels, G.C. Cho, T. Dekorsy, H. Kurz, A. Stahl, K. Köhler, Phys. Rev. B **55**, 16404 (1997).
17. V. Chernyak, S. Yokojima, T. Meier, S. Mukamel, Phys. Rev. B **58**, 4496 (1998).
18. S. Bar-Ad, I. Bar-Joseph, Phys. Rev. Lett. **68**, 349 (1992); G. Finkelstein, S. Bar-Ad, O. Carmel, I. Bar-Joseph, Y. Levinson, Phys. Rev. B **47**, 12964 (1993).
19. E. Runge, R. Zimmermann, Phys. Stat. Sol. B **206**, 167 (1998).
20. J.J. Sanchez-Mondragon, N.B. Narozhny, J.H. Eberly, Phys. Rev. Lett. **51**, 550 (1983).
21. D. Meschede, H. Walther, G. Müller, Phys. Rev. Lett. **54**, 551 (1985); M.G. Raizen, R.J. Thompson, R.J. Brecha, H.J. Kimble, H.J. Carmichael, Phys. Rev. Lett. **63**, 240 (1989); Y. Zhu, D.J. Gauthier, S.E. Morin, Q. Wun, H.J. Carmichael, T.W. Mossberg, Phys. Rev. Lett. **64**, 2499 (1990).
22. C. Weisbuch, M. Nishioka, A. Ishikawa, Y. Arakawa, Phys. Rev. Lett. **69**, 3314 (1992); R. Houdre, C. Weisbuch, R.P. Stanley, U. Oesterle, P. Pellandini, M. Ilegems, Phys. Rev. Lett. **73**, 2043 (1994).
23. F. Jahnke, M. Kira, S.W. Koch, G. Khitrova, E.K. Lindmark, T.R. Nelson Jr., D.V. Wick, J.D. Berger, O. Lyngnes, H.M. Gibbs, K. Tai, Phys. Rev. Lett. **77**, 5257 (1996).

24. O. Lyngnes, J.D. Berger, J.P. Prineas, S. Park, G. Khitrova, H.M. Gibbs, F. Jahnke, M. Kira, S.W. Koch, Solid State Commun. **104**, 297 (1997); F. Jahnke, M. Kira, S.W. Koch, Z. Phys. B **104**, 559 (1997); G. Khitrova, H.M. Gibbs, F. Jahnke, M. Kira, S.W. Koch, Rev. Mod. Phys. (Oct. 1999).
25. H. Wang, J. Shah, T.C. Damen, W.Y. Jan, J.E. Cunningham, M. Hong, J.P. Mannaerts, Phys. Rev. B **51**, 14713 (1995).
26. M. Koch, J. Shah, T. Meier, Phys. Rev. B **57**, R2049 (1998).
27. X. Fan, H. Wang, H.Q. Hou, B.E. Hammons, Phys. Rev. B **57**, R9451 (1998).
28. W. Huhn, A. Stahl, Phys. Stat. Sol. B **124**, 167 (1984).
29. H. Haug, S.W. Koch, *Quantum Theory of the Optical and Electronic Properties of Semiconductors*, 3rd edn. (World Scientific, Singapore, 1994).
30. T. Stroucken, A. Knorr, P. Thomas, S.W. Koch, Phys. Rev. B **53**, 2026 (1996).
31. L. Banyai, I. Gailbraith, C. Ell, H. Haug, Phys. Rev. B **36**, 6099 (1987).
32. K. Bott, J. Hader, S.W. Koch, P. Thomas, Phys. Rev. B **56**, 12784 (1997).
33. D. Brinkmann, K. Bott, S.W. Koch, P. Thomas, Phys. Stat. Sol. B **206**, 493 (1998).
34. It has been checked that all features present in the numerical results do not change for larger systems.
35. M. Lindberg, R. Binder, S.W. Koch, Phys. Rev. A **45**, 1865 (1992).
36. S.W. Koch, N. Peyghambarian, M. Lindberg, J. Phys. C **21**, 5229 (1988).
37. M. Kira, F. Jahnke, S.W. Koch, Solid State Commun. **102**, 703 (1997).
38. S. Mukamel, *Principles of Nonlinear Optical Spectroscopy* (Oxford, New York, 1995); T. Meier, V. Chernyak, S. Mukamel, J. Chem. Phys. **107**, 8759 (1997).
39. In reference [3] the unbound two-exciton states have been treated within the Markov and second-order Born-approximations. In the simple model considered in the Appendix we instead take for B^{1111} and B^{2222} a single unbound two-exciton state explicitly into account. This state serves as a representative of the two-exciton continuum.
40. M. Wegener, D.S. Chemla, S. Schmitt-Rink, W. Schäfer, Phys. Rev. A **42**, 5675 (1990).
41. R. Zimmermann, Phys. Stat. Sol. B **159**, 317 (1990).
42. R. Binder, S.W. Koch, M. Lindberg, W. Schäfer, F. Jahnke, Phys. Rev. B **43**, 6520 (1991).
43. Similar correlation-type contributions, *i.e.* bleaching at the exciton resonance and excited-state absorption due to the presence of two-excitons are also found in aggregates of Frenkel excitons, see *e.g.* reference [44].
44. T. Meier, V. Chernyak, S. Mukamel, J. Phys. Chem. B **101**, 7332 (1997); W.M. Zhang, T. Meier, V. Chernyak, S. Mukamel, J. Chem. Phys. **108**, 7763 (1998).